The role of the anisotropy on the solid-fluid phase transition in core-softened shoulder-dumbbells systems

Cristina Gavazzoni[1],Guilherme K. Gonzatti[2], Luiz Felipe Pereira[1],Luis Henrique Coelho Ramos[1], Paulo A. Netz[2], Marcia C. Barbosa[1]

[1] *Instituto de Física, Universidade Federal do Rio Grande do Sul, Porto Alegre, RS, 91501-970, Brazil.*

[2] *Instituto de Química, Universidade Federal do Rio Grande do Sul, Porto Alegre, RS, 91501-970, Brazil.*

(Dated: March 29, 2014)

Abstract

Using molecular dynamics we studied the role of the anisotropy on the phase boundary of 250 dimeric particles interacting by a core-softened potential. This study led us to an unexpected result: the introduction of a rather small anisotropy, quantified by the distance between the particles inside each dimer, leads to an apparent increase of the size of the solid region in the pressure-temperature phase diagram when compared to the isotropic monomeric case. However, as the anisotropy increases beyond a threshold the solid region shrinks. We found that this behavior can be understood by the decoupling of the translational and non-translational kinetic energy components that could be interpreted as if the system would display different translational and non-translational temperatures. The phase boundaries seems to be sensitive to the translational temperature only.

I. INTRODUCTION

There are liquids in nature that exhibit unexpected thermodynamic or transport properties. Water belongs in this group of anomalous liquids and it is the one with the most puzzling behavior. It expands upon cooling at fixed pressure (density anomaly), diffuses faster upon compression at fixed temperature (diffusion anomaly) and become less ordered upon increasing density at constant temperature (structural anomaly). Despite the complexity of its anomalies, simple molecular water models proved to be able to reproduce many of water unusual properties [1–3].

The origin of water's anomalies is related to the competition between open low-density and closed high-density structures, which depend on the thermodynamic state of the liquid [4]. With the purpose of understanding the nature of these anomalies several models were proposed in which spherically symmetric particles interact with each other by an isotropic potential [5–30] where this competition is described by two preferred interparticle distances.

Among these models, the core-softened shoulder potential proposed by Oliveira *et. al.*[21, 22] reproduces qualitatively some of the most remarkable water's anomalies. In particular the regions of density anomaly, diffusion anomaly and structural anomaly obey the same hierarchy as found in real water [1]. This potential can represent in an effective and orientation-averaged way the interactions between water clusters characterized by the presence of those two structures (open and closed) discussed above. The open structure is favored by low pressures and the closed structure is favored by high pressures, but only becomes accessible at sufficiently high temperatures.

Even though core-softened potentials have been mainly used for modeling water [12, 21, 22, 26, 30–34], many other materials present the so called water-like anomalous behavior[3, 35–41] and, in principle, could be represented by two length potentials. In this sense, it is reasonable to use core-softened potentials as the building blocks of a broader class of materials which we can classify as anomalous fluids. Despite the success of these models some properties are not well represented by spherical symmetric potentials. As recently reviewed by Vilaseca and Franzese,[42], isotropic core-softened potentials fail to describe the correct P-dependence of structural fluctuations[42], affecting some properties such as the velocity of sound and the compressibility, in the supercooled state and at ambient temperature.

In a recently study we compared the monomeric model proposed by Oliveira *et. al.*[21, 22]

with a model of dimeric molecules linked as rigid dumbbells, interacting with the same potential. The introduction of anisotropy leads to a much larger region of solid phase in the phase diagram and to the appearance of a liquid crystal phase[43]. Later we showed that the size of anomalous regions in the pressure temperature phase diagram is dependent on the distance of the particles belonging to the same dimers and that the effect of the introduction of a rather small anisotropy due to the dimeric nature of the particle leads to the increase of the size of the regions of anomalies. Nevertheless, the increase of interparticle separation shrinks those regions [44].

In the present work we will show that a possible explanation for this unexpected behavior is that, in conditions of low temperature and pressure, there is a decoupling of translational and rotational degrees of freedom when the interparticle separation is small. Experimental works showed that when approaching the glass transition the translational and rotational dynamics are not equally affected [45, 46]. This behavior was also observed in computer simulations [47].

In order to test this hypothesis here we study a dimeric model where each particle in the dimer interacts with the particles in the other dimers through a core-softened potential. We define translational and non-translational temperatures as tools to evaluate the role of translational and non-translational degrees of freedom. Different values of the interparticle separation λ were used and compared.

The remaining of this manuscript goes as follows. In Sec. II the model is introduced and the simulation details are presented. In Sec. III the results are shown and conclusions are exposed in Sec. IV.

II. THE MODEL

Our model consists of N spherical particles of diameter σ, linked rigidly in pairs with the distance λ between their centers of mass forming dimers as shown in figure 1. In this way, $\lambda^* \equiv \lambda/\sigma$ is related to the anisotropy of the dimers. Each particle of the dimer interacts with all particles belonging to other dimers with the intermolecular continuous shoulder potential [21, 43] given by

$$U^*(r) = \frac{U(r)}{\epsilon} = 4\left[\left(\frac{\sigma}{r}\right)^{12} - \left(\frac{\sigma}{r}\right)^{6}\right] + a\exp\left[-\frac{1}{c^2}\left(\frac{r-r_0}{\sigma}\right)^2\right] . \quad (1)$$

Depending on the choice of the values of a, r_0 and c a whole family of potentials can be built, which shapes ranging from a deep double wells[20, 35] to a repulsive shoulder[16]. In our simulations we used $a = 5$, $r_0/\sigma = 0.7$, $c = 1$ and $\lambda^* = 0.10, 0.20, 0.50$ and 0.70.

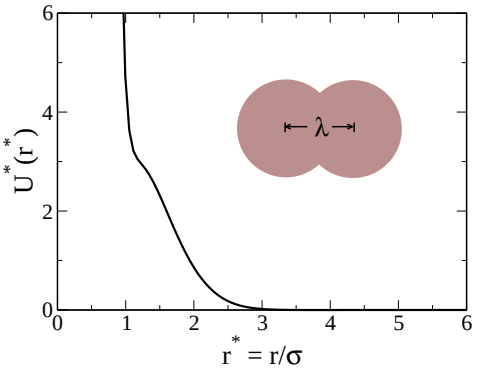

FIG. 1: Effective potential versus distance in reduced units.

We performed molecular dynamics simulations in the canonical ensemble using $N = 500$ particles (250 dimers) in a cubic box of volume V with periodic boundary conditions in three directions, interacting with the intermolecular potential described above. The cutoff radius was set to 5.5σ length units. Pressure, temperature, density and diffusion are calculated in dimensionless units

$$T^* \equiv \frac{k_B T}{\epsilon}$$

$$\rho^* \equiv \rho\sigma^3$$

$$P^* \equiv \frac{P\sigma^3}{\epsilon}$$

$$D^* \equiv \frac{D(m/\epsilon)^{1/2}}{\sigma}$$

$$t^* \equiv t\left(\frac{\varepsilon}{m\sigma^2}\right)^{1/2}$$

In order to test the dependence of our results with the size of the system we also carried out simulations with 1000 (500 dimers) and with 2000 (1000 dimers) particles for $\lambda^* = 0.20$. The results obtained were essentially the same as the results obtained with 500 (250 dimers) particles [43].

Thermodynamic and dynamic properties were calculated over 1000000 steps after previous 300000 equilibration steps. The time step was 0.001 in reduced units, the time constant of the Berendsen thermostat [48] was 0.1 in reduced units. The internal bonds between the particles in each dimer remain fixed using the algorithm SHAKE [49] with a tolerance of 10^{-12} and maximum of 100 interactions for each bond. For a set of points we also carried out simulations two times longer with essentially the same results [50].

The structure of the system was characterized using the intermolecular radial distribution function, $g(r)$ (RDF), which does not take into account the correlation between particles belonging to the same dimers and the slope of the least square fit to the linear part of the mean square displacement, $< r^2(t) >$ (MSD). Both the $g(r)$ and $< r^2(t) >$ where computed relative to the center of mass of a dimer. The phase boundary between the solid and fluid phases was mapped by the analysis of the change of the pattern of mean square displacement and radial distribution function [44].

In a previous work [43] we showed that, depending on the chosen temperature and density, the system could be in a fluid phase metastable with respect to the solid phase. In order to locate the phase boundary two sets of simulations were carried out, one beginning with molecules in a ordered crystal structure and other beginning with molecules in a random, liquid, starting structure obtained from previous equilibrium simulations.

The dynamic of the system was analyzed through the mean square displacement (which allows to calculate the diffusion coefficient) and the velocity and orientational autocorrelation functions. The velocity autocorrelation function is calculated taking the average for all dimers and initial times through the expression

$$v_{acf}(t) = \langle \mathbf{v}_i(t_0) \cdot \mathbf{v}_i(t_0 + t) \rangle \tag{2}$$

where $\mathbf{v}_i(t_0)$ is the initial velocity vector for the dimer i and $\mathbf{v}_i(t_0 + t)$ is the velocity vector for the same dimer at a later time $t_0 + t$. The orientational autocorrelation function is defined by

$$O^{l}_{acf}(t) = \langle P_l(cos\theta_i)\rangle \tag{3}$$

where P_l is the Legendre polynomial of order l and θ_i is the reorientation angle of the intra-dimer vector during the time interval Δt. In our case, we calculate only the first order correlation $l = 1$, which is equivalent to $O^{l}_{acf}(t) = \langle \mathbf{e}_i(t_0) \cdot \mathbf{e}_i(t_0 + t)\rangle$ where $\mathbf{e}_i$ is the main axis vector of the dimer i. We will omit the order of the correlation in the results section.

III. RESULTS

A. P-T phase diagram for different values of λ^*

In previous work [43, 44], we studied a system of 250 dimers, interacting through the interparticle potential (1) with $\lambda^* = 0.20$ [43], 0.10, 0.50 and 0.70 [44] in a broad range of densities and temperatures. The pressure, radial distribution function, mean square displacement and diffusion coefficient were calculated for all state points, yielding a complete description of the regions of structural, density and diffusion anomalies.

The comparison between the monomeric case and the dimeric cases with $\lambda^* = 0.20$[43] or $\lambda^* = 0.10$, 0.50 and 0.70[44] showed in the pressure vs temperature phase diagram that the anisotropy due the dumbbells leads to larger range of pressures and temperatures occupied by anomalous regions and by the solid phase. In this publications in order to carry out this comparison for various λ^* values with the monomeric case, we scaled the phase diagram of dimers by a factor of 0.25 because a hypothetical dimer with interparticle distance $\lambda^* = 0$ would interact with another similar dimer with a potential energy equivalent to two monomers in one position interacting with two monomers in the other position, which means an interaction four times stronger. We could also rescale solid-fluid phase transition boundary for the monomeric case by a factor of 4, or we could alternatively apply another kind of scaling such as the Noro-Frenkel generalized law of correspondent states [51] which was also extended to anisotropic systems [52]. However, those approches are not appropriated for our case, since we want to compare the monomeric with the dimeric case in the melting line region, where the second virial is not a good approximation for the equation of state. In addition, this extended NFLCS works very well for patchy systems, where the interaction between molecules is strongly dependend on the angle between the main axis

of the dimer and the intermolecular particle-particle axis. In our case, the anisotropy has a very different nature, with each monomer inside each dimer interacting with every other monomers belonging to other dimers, notwithstanding their relative angular orientation.

The pressure versus temperature phase diagram for the $\lambda^* = 0.20$ and 0.50 systems obtained in the previous works show that the solid-fluid phase boundary and the TMD are shifted towards lower temperatures and slightly higher pressures with the increase of λ^* for all the cases. This result is consistent with the idea that increasing the anisotropy leads to a higher entropy and lower temperature of the melting. The high-temperature limit of the boundary of the region of diffusion anomalies also becomes shifted towards lower temperatures, whereas the lower-temperature part of this region becomes broader. The structurally anomalous region shrinks with increasing λ^*.

Simulation studies using core-softened potentials showed that the increase of the repulsive shoulder width moves the solid-fluid phase transition and the region of density and diffusion anomalies to lower temperatures [53–56]. Thus it is reasonable to say that in some sense the increase of the interparticle separation of dimeric systems may be considered as similar to the increase of the repulsive shoulder width of the effective isotropic potential between the dimeric particles averaged over rotations.

In order to confirm the influence of λ^* on the phase diagram and regions of anomalous behavior, here we performed several simulations exploring the densities between $\rho^* = 0.10$ and $\rho^* = 0.30$ and the temperatures between $T^* = 0.10$ and $T^* = 0.80$ for several values of interparticle separation $\lambda^* = 0.10, 0.20, 0.50$ and 0.70 complementary to the simulations alredy discussed in [44]. Figure 2 shows the solid-fluid phase boundary in the pressure temperature phase diagram for $\lambda^* = 0.10, 0.20, 0.50$ and 0.70 and also for the monomeric case, where both temperature and pressure were rescaled by a factor of 4. We also run simulations for $\lambda^* = 0.02$ and $\lambda^* = 0.01$ but for systems with very small interparticle separations the equilibrium was not reached. The figure shows that the increase of the interparticle separation shifts the solid-fluid phase boundary to lower temperatures.

Comparing the results of the simulations corresponding to the several values of λ^* we observe that the melting line temperature decreases with the increase of the value of interparticle separation λ^* for all systems. A non-monotonic behavior is observed instead of having the monomeric case as the limit of $\lambda^* \to 0$. In order to check why as $\lambda^* \to 0$, the system does not converge to the monomeric case, the orientational degrees of freedom were

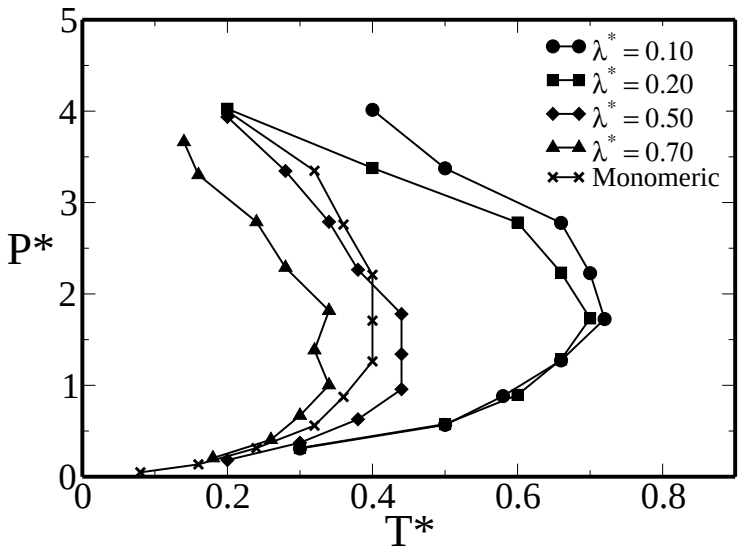

FIG. 2: Solid-fluid phase boundary for different values of interparticle separation λ^* and for monomeric case[21, 22] rescaled by a factor of 4.

analyzed.

Autocorrelation functions are very powerful tools to describe dynamics, therefore the analysis of these curves may give us an idea why the solid-fluid phase boundary is contracting with the increase of λ^*. Fig. 3 shows the velocity autocorrelation functions, $v_{acf}(t)$, the orientational autocorrelation function, $O_{acf}(t)$, and mean square displacement, $< r^2(t) >$, for simulations with different values of λ^* subject to the same conditions of density and temperature.

The velocity autocorrelation function v_{acf} versus time, illustrated in Fig. 3(a) and (b), shows that for all the values of λ^* the curves present a fast decay, however, only the curves for small interparticle separation λ^* cross the zero axis at short time. This result indicate that the less anisotropic particles (small λ^*) "feel" the cage of neighbors molecules more strongly than the more anisotropic particles. With the increase of the temperature this effect is weakened, consequently the behavior of v_{acf} for $\lambda^* = 0.10$ and $T^* = 0.50$ is similar to the behavior of $\lambda^* = 0.20$ and $T^* = 0.30$. Therefore the increase of the temperature compensates the decrease of the λ^* value.

The slope of mean square displacement, illustrated in Fig. 3, is related with the translational diffusion. As exemplified for density $\rho^* = 0.30$ and $T^* = 0.30$, the larger the interparticle separation, λ^*, the larger is the translational diffusion of the system. With the

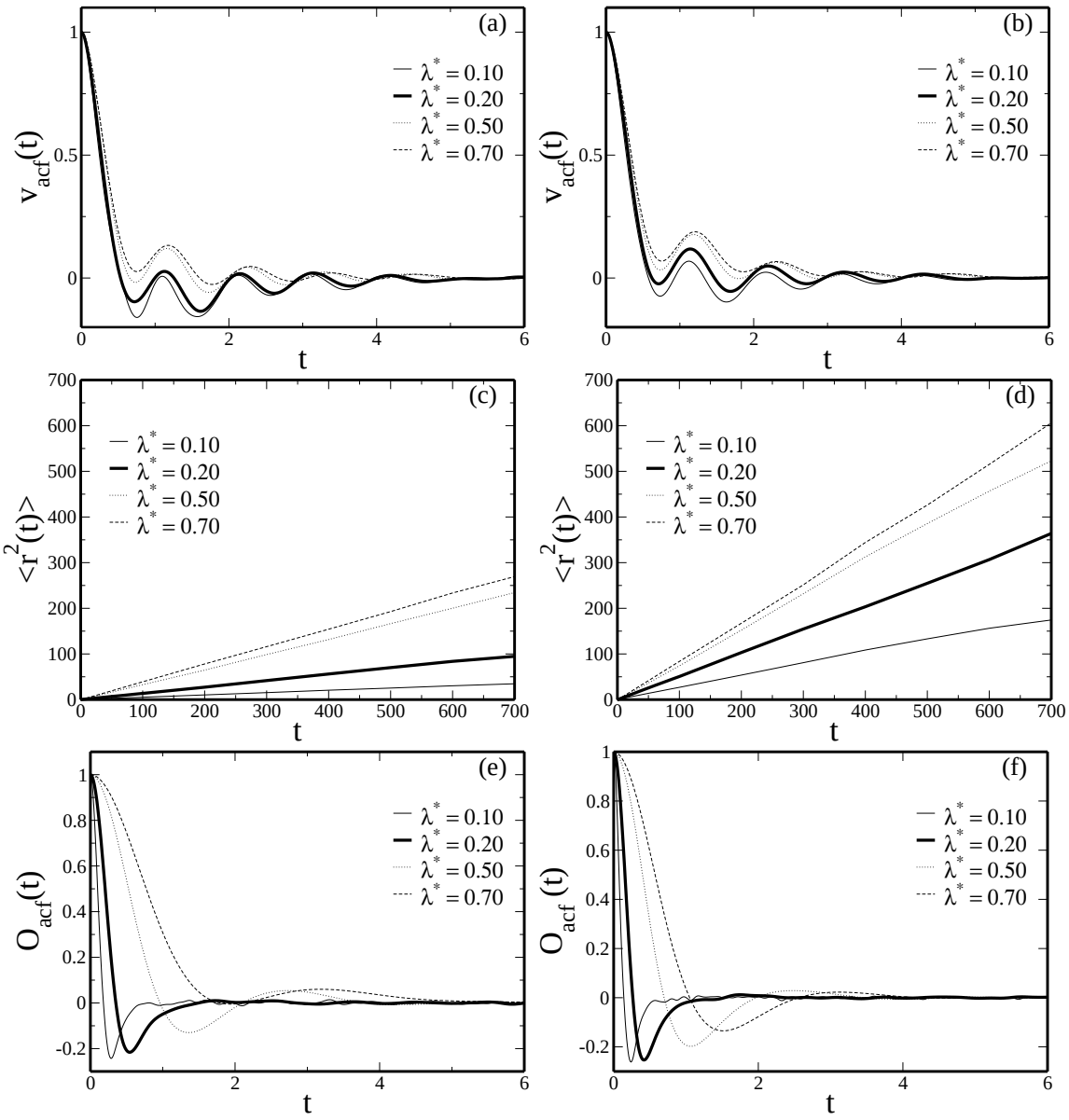

FIG. 3: Velocity autocorrelation function, $v_{acf}(t)$ for (a)$T^* = 0.30$ and (b)$T^* = 0.50$, mean square displacement, $< r^2(t) >$ for (c)$T^* = 0.30$ and (d)$T^* = 0.50$, and orientational autocorrelation function, $O_{acf}(t)$ for (e)$T^* = 0.30$ and (f)$T^* = 0.50$. All the graphs are for $\rho^* = 0.30$.

increase of the temperature all systems become more diffusive. However, the largest change occurs for the small values of λ^* .

The orientational autocorrelation function, O_{acf}, is also shown in the Fig. 3. The less anisotropic systems for $\rho^* = 0.30$ and $T^* = 0.30$ have a O_{acf} that decays quickly to zero. This result indicates that, for these systems, the time needed to perform a 90^o rotation is

very small, i.e., systems with small interparticle separation rotate much easier then systems with larger λ^* values. For all the interparticle separations, λ^*, the orientational mobility is facilitated by the increase of the temperature. It is noteworthy that the differences in O_{acf} (Fig. 3(e) e Fig. 3(f)) are much more pronounced that the difference in v_{acf} (Fig. 3(a) e Fig. 3(b)).

The analysis of the behavior of $< r^2(t) >$, v_{acf} and O_{acf} for several values of λ^*, ρ^* and T^* leads to the conclusion that the more anisotropic systems (larger λ^*)) diffuse faster but rotate slower than systems with low anisotropy (small λ^*). Based on these observation we raised the hypothesis that the shrinking of the region of solid phase is related to a decoupling between translational and non-translational motions.

In order to test our hypothesis we defined a translational temperature and a non-translational temperature as tools to evaluate the role of translational and non-translational degrees of freedom.

B. Translational and non-translational temperatures

In our dimeric system simulations, as well as in our monomeric simulations [21, 22], Berendsen thermostat is used to maintain the temperature fixed. In this thermostat the velocities are periodically rescaled so that the actual temperature of the system, which is defined as the kinetic energy of the system divided by the number of degrees of freedom, relaxes toward a chosen system temperature (formal temperature). When we are dealing with monomeric systems the temperature has only the contribution of the translational kinetic energy but for dimeric systems, the temperature has the translational plus the rotational (and eventually vibrational) kinetic energy contributions. In another words, due to its rotational or vibrational kinetic energy, a dimeric particle rotating or vibrating around a single point has a non zero temperature, even though its center of mass remains still. Since the dimeric system is composed by hard-linked particles the internal vibration is excluded, remaining only the rotational and hindered rotational (libration) motions.

In order to test the effect in the pressure versus temperature phase diagram of the decoupling of the temperature we calculated separately the contributions of translational movement, which we associate with a translational temperature, and non-translational movement, associated with a non-translational temperature. Each degree of freedom contribute with

$k_BT/2$ to the kinetic energy.

The contributions of total kinetic energy were obtained calculating the kinetic energy of each monomer in the system, namely

$$K = f\frac{k_BT}{2} = 5\frac{N}{2}\frac{k_BT}{2} \tag{4}$$

where the temperature T is the temperature fixed by the thermostat. This total energy can be separated into two terms: the kinetic energy of the translational modes and the kinetic energy of the non-translational modes. These two modes in general are coupled and, therefore, the translational and non translational modes are related to the same temperature. This, however, is not the case for a number of systems as, for example, the plastic phases [57, 58]. In these cases, the translation and rotation can be excited in a very different way.

The contributions for the translational kinetic energy is given by the kinetic energy of the center of mass of the dimeric particles, K_{trans}. Thus if the dimeric particle is rotating around a single point the translational contribution will be zero. In the general case, since there are $N/2$ dimers, the kinetic energy is related to the translational temperature by the definition

$$K_{trans} = 3\frac{N}{2}\frac{k_BT_{trans}}{2} \tag{5}$$

where T_{trans} is the translational temperature. Non-translational temperature was also defined using the equipartition theorem. The non-translational contributions of internal energy is

$$K_{ntrans} = 2\frac{N}{2}\frac{k_BT_{ntrans}}{2} = \frac{N}{2}k_BT_{ntrans} \tag{6}$$

where T_{ntrans} is the non-translational temperature. Using this equation and considering $K = K_{trans} + K_{ntrans}$ we can write an expression for the non-translational temperature

$$T_{ntrans} = \frac{5}{2}T - \frac{3}{2}T_{trans} \tag{7}$$

When translation and rotation are equaly excited this would imply that $T_{trans} = T_{ntrans}$ and the expression above would be an identity. But, as we are going to see, in our systems this is not the case depending on the value of the λ^*. Using this approach we analyzed the influence of interparticle separation on the decoupling between translational and

non-translational motion. Figure 4 shows T^*_{trans} vs T^*_{ntrans} comparing different values of λ^* for several densities. We see that $T^*_{ntrans} \geq T^*_{trans}$. For small λ^*, a linear behavior $T^*_{trans} = a(\rho)T^*_{ntrans}$ is observed but only for a certain interval of densities. As the density increases $a(\rho) \to 1$. According to the definitions described above, this means that, for small interparticle separation, the system can easily perform a non-translational motion without performing a translational one. As the density and the total temperature increase the motions of the system become more correlated. For higher values of λ^* the decoupling is not observed. In this case, for all densities $T^*_{trans} = T^*_{ntrans}$. In these cases the non-translational motion is strongly dependent (coupled) on translational motion. For a deeper analysis of the

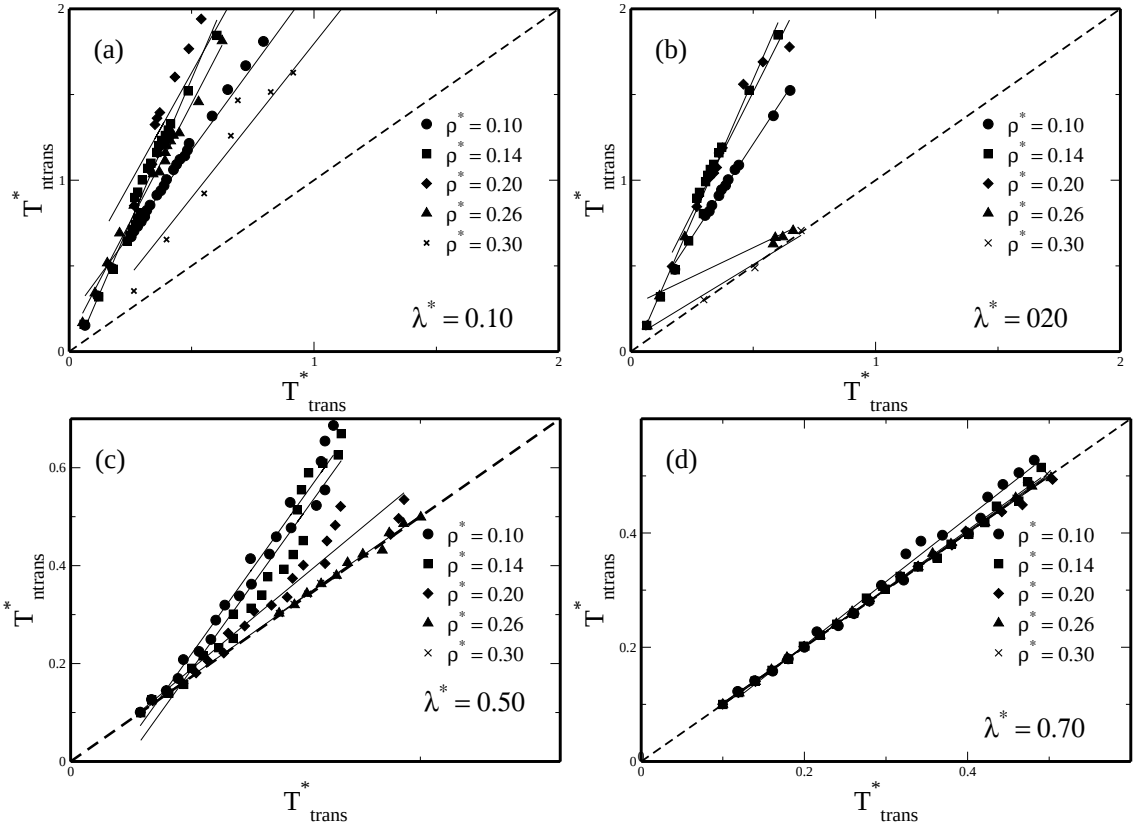

FIG. 4: Translational temperature vs non-translational temperature for $(a)\lambda^* = 0.10, (b)\lambda^* = 0.20, (c)\lambda^* = 0.50$ and $(d)\lambda^* = 0.70$. In each case results with $\rho^* = 0.10, 0.14, 0.20, 0.26$ and 0.30 are shown.

effects linked to the different degrees of freedom we rescaled the pressure temperature phase diagram using the translational and non-translational temperature. Figure 5 shows the rescaled solid-fluid phase boundary with respect the translational temperature for various

values of λ^*. The melting line for all interparticle separation moves backwards in temperature. However, when we rescale the phase boundary with non-translational function (not shown) we could observe the opposite behavior: The curves moves forth in temperature.

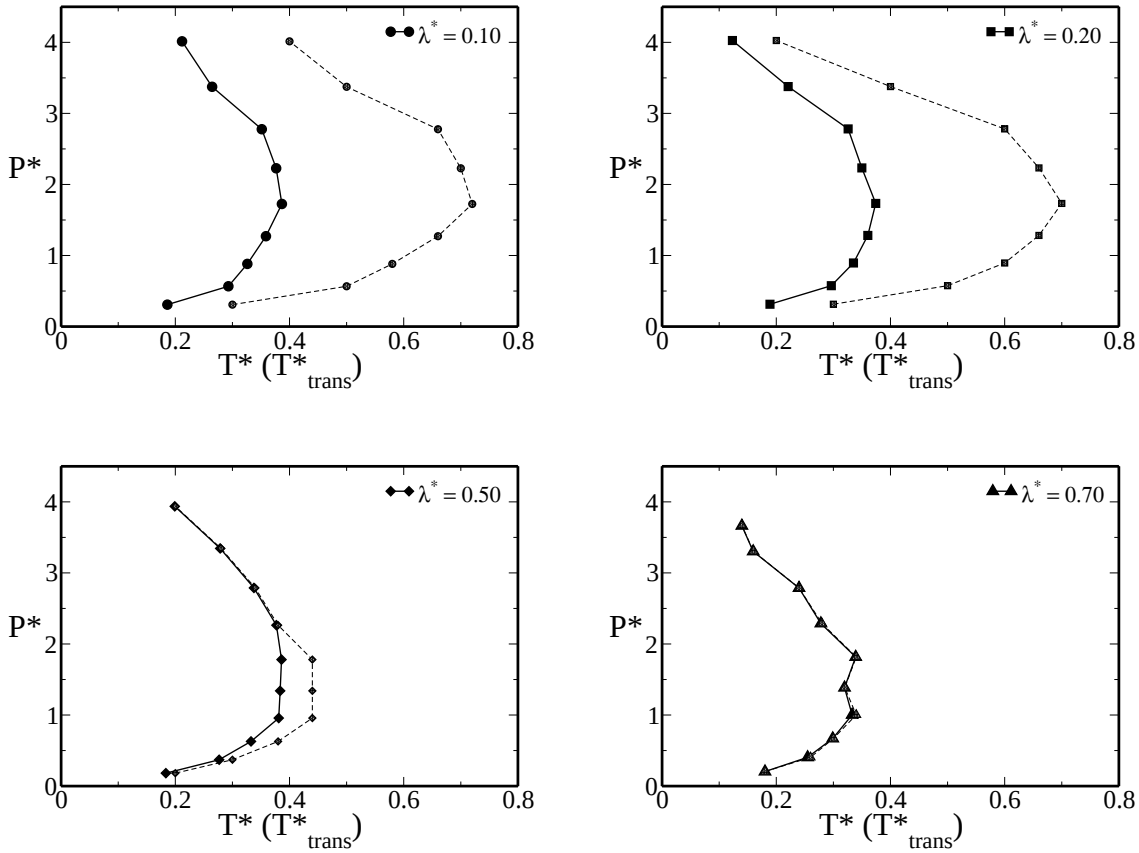

FIG. 5: Solid-fluid phase boundary for different λ^*. The solid lines represent the solid-fluid phase boundary rescaled with translational temperature, the dashed lines represent the original phase boundary.

The behavior of the solid-fluid boundary, as well as the anomalous region in the pressure-temperature phase diagram are, in fact, sensitive to translational temperature. Indeed, in systems where molecules are able to perform non-translational movements without perform translational ones, as in the case of small λ^*, the dimers interacts with the other dimers in such a way that their center of mass stay ordered in a solid lattice, despite of the non-zero non-translational kinetic energy. Thus, the translational temperature acts like the true effective temperature.

Systems with smaller interparticle separation λ^* present a larger difference between the translational temperature and the formal temperature than systems with larger λ^*, due to the decoupling of translational and non-translational degrees of freedom. This difference is responsible for the apparent non-monotonic behavior of the region of solid phase.

In order to highlight the effects due to the translational degrees of freedom, figure 6 shows the solid-fluid phase boundary rescaled using the translational temperature for several λ^* and the solid-fluid phase boundary for the monomeric system. We can observe that, taking into

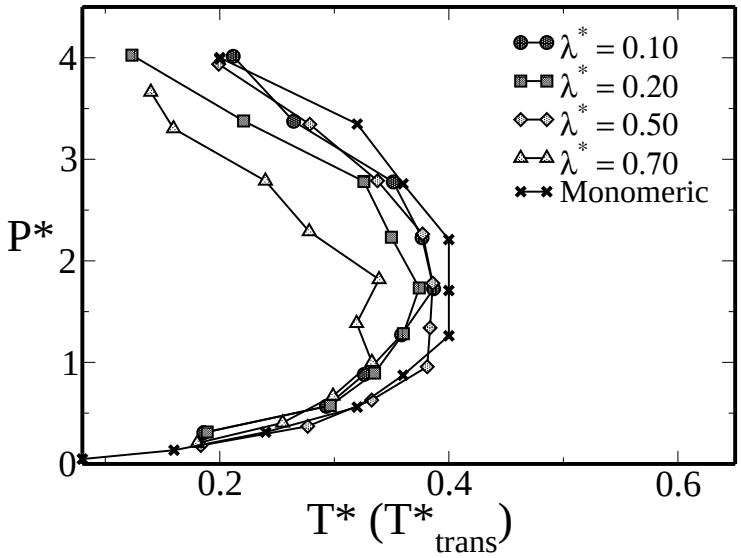

FIG. 6: Solid-fluid phase boundary for different λ^* rescaled with translational temperature and Solid-fluid phase boundary for the monomeric system rescaled by a factor of 4.

account only translational movements, the introduction of an anisotropy makes the region of solid phase move slightly backwards in temperature. We also observe that the curves corresponding to $\lambda^* = 0.10, 0.20$ and 0.50 almost collapsed in one region indicating that the solid-fluid phase boundary depends effectively on the translational part of the temperature. Small dimeric particles can easily perform a non-translational motion and therefore, in some state points where the rotational kinetic energy is high enough, could behave as a solid, despite having a formal high temperature, due to their low translational temperature. Therefore the unexpected non-monotonic behavior is indeed due to the non-translational motion as predicted by our hypothesis.

The phase boundary for $\lambda^* = 0.70$ does not collapses like the other ones. The reason behind this observation remains still an open question, but maybe is related to the effective

higher anisotropy of this system. Nevertheless, despite of $\lambda^* = 0.70$ we can affirm that the non-monotonic behavior is essentially due the difference between translational temperature and the formal temperature.

IV. CONCLUSION

We performed molecular dynamics with rigid dimers, in which each monomer interacts with monomers from other dimers through a core-softened shoulder potential, in order to study the influence of anisotropy in anomalous regions and solid-fluid phase boundary. We carried out simulations for interparticle separation $\lambda^* = 0.10, 0.20, 0.50$ and 0.70 and we observed an unexpected non-monotonic behavior where the solid phase shrinks with increase of λ^*.

Through the analysis of velocity and orientational autocorrelation functions and the mean square displacement we formulated a hypothesis that decoupling between translational and non-translational motion would be responsible for the shrinking of the region of solid phase in the phase diagram.

In order to test these assumption we defined translational and non-translational temperatures, obtained from the kinetic energy, as tools to evaluate the role of translational and non-translational degrees of freedom. We obtained that for simulations with small values of λ^* the non-translational temperature is much higher than the translational temperature. For larger values of λ^* the temperatures are correlated independently of density and temperature. These results are consistent with the non-monotonic behavior observed.

We rescaled the pressure-temperature phase diagram in order to obtain a pressure versus translational temperature phase diagram and observed the behavior of solid phase. We argue that translational temperature is the proper effective temperature for understanding what happens with the translational movement of the system. The non-monotonic behavior of solid-fluid phase boundary is, therefore, due to the difference between translational temperature and the actual temperature. We observed that the introduction of anisotropy leads to a smaller region in the pressure-temperature phase diagram of the solid phase when compared with monomeric system and that the solid-fluid phase boundary for $\lambda^* = 0.10, 0.20$ and 0.50 collapsed on one region of phase diagram when only the translational modes are taken into account.

Despite of that we still have open questions since the phase boundary for $\lambda^* = 0.70$ did not collapsed like the others. The reason behind that could be related to the size of the dimer. Nevertheless we succeeded to explain most part of the reasons that led to the non-monotonic behavior of solid-fluid boundary which lead us one step forward in the understanding of more complex systems.

V. ACKNOWLEDGMENTS

We thank Brazilian science agency CNPq for financial support.

[1] P. A. Netz, F. W. Starr, H. E. Stanley and M. C. Barbosa, J. Chem. Phys.**115**, 344 (2001).

[2] J. R. Errington and P.D. Debenedetti, Nature (London) **409**, 318 (2001).

[3] C. A. Angell, R. D. Bressel, M. Hemmatti, E. J. Sare and J. C. Tucker, Phys. Chem. Chem. Phys. **2**, 1559 (2000).

[4] W. P. Krekelberg, J. Mittal, V. Ganesan and T. M. Truskett, Phys. Rev. E **77**, 041201 (2008).

[5] A. Scala, M. R. Sadr-Lahijany, N. Giovambattista, S. V. Buldyrev, and H. E. Stanley, J. Stat. Phys. **97**, 100 (2000).

[6] G. Franzese, Malescio, A. Skibinsky, S. V. Buldyrev and H. E. Stanley, Nature (London) **409**, 692 (2001).

[7] S. V. Buldyrev, G. Franzese, N. Giovambattista, G. Malescio, M. R. Sadr-Lahijany, A. Scala, A. Skibinsky, and H. E. Stanley, Physica A **304**, 23 (2002).

[8] S. V. Buldyrev and H. E. Stanley, Physica A **330**, 124 (2003).

[9] A. Skibinsky, S. V. Buldyrev, G. Franzese, G. Malescio and H. E. Stanley, Phys. Rev. E **69**, 061206 (2005.

[10] G. Franzese, G. Malescio, A. Skibinsky, S. V. Buldyrev and H. E. Stanley, Phys. Rev. E **66**, 051206 (2002).

[11] A. Balladares and M. C. Barbosa, J. Phys.: Cond. Matter **16**, 8811 (2004).

[12] A. B. de Oliveira and M. C. Barbosa, J. Phys.: Cond. Matter **17**, 399 (2005).

[13] V. B. Henriques and M. C. Barbosa, Phys. Rev. E **71**, 031504 (2005).

[14] V. B. Henriques, N. Guissoni, M. A. Barbosa, M. Thielo and M. C. Barbosa, Mol. Phys. **103**, 3001 (2005).

[15] P. C. Hemmer and G. Stell, Phys. Rev. Lett. **24**, 1284 (1970).

[16] E. A. Jagla, Phys. Rev. E **58**, 1478 (1998).

[17] N. B. Wilding and J. E. Magee, Phys. Rev. E **66**, 031509 (2002).

[18] R. Kurita and H. Tanaka, Science **306**, 845 (2004).

[19] L. Xu, P. Kumar, S. V. Buldyrev, S. -H. Chen, P. Poole, F. Sciortino and H. E. Stanley, Proc. Natl. Acad. Sci. U.S.A. **102**, 16558 (2005).

[20] P.A. Netz, J. F. Raymundi, A. S. Camera and M. C. Barbosa, Physica A **342**, 48 (2004).

[21] A. B. de Oliveira, P. A. Netz, T. Colla and M. C. Barbosa, J. Chem. Phys. **124**, 084505 (2006).

[22] A. B. de Oliveira, P. A. Netz, T. Colla and M. C. Barbosa, J. Chem. Phys. **125**, 124503 (2006).

[23] A. B. de Oliveira, M. C. Barbosa and P. A. Netz, Physica A **386**, 744 (2007).

[24] A. B. de Oliveira, P. A. Netz, and M. C. Barbosa, European Physics Journal B **64**, 481 (2008).

[25] A. B. de Oliveira, G. Franzese, P. A. Netz, and M. C. Barbosa, J. Chem. Phys. **128**, 064901 (2008).

[26] A. B. de Oliveira, P. A. Netz and M. C. Barbosa, Euro. Phys. Lett **85**, 36001 (2009).

[27] Yu. D. Fomin, N. V.Gribova, V. N. Ryzhov, S.M. Stishov and D. Frenkel, J. Chem. Phys. **129**, 064512 (2008).

[28] N. G. Almarza, J. A. Capitan, J. A. Cuesta and E. Lomba, J. Chem. Phys. **131**, 124506 (2009).

[29] M. Pretti and C. Buzano, J. Chem. Phys. **121**, 11856 (2004).

[30] H. M. Gibson and N. B. Wilding, Phys. Rev. E **73**, 061507 (2006).

[31] L. Xu, S. Buldyrev, C. A. Angell and H. E. Stanley, Phys. Rev. E **74**, 031108 (2006).

[32] Z. Yan, S. V. Buldyrev, N. Giovambattista and H. E. Stanley, Phys. Rev. Lett. **95**, 130604 (2005).

[33] Z. Yan, S. V. Buldyrev, N. Giovambattista, P. G. Debenedetti and H. E. Stanley, Phys. Rev. E **73**, 051204 (2006).

[34] G. Franzese, J. Mol. Liq. **136**, 267 (2007).

[35] H. Thurn and J. Ruska, J. Non-Cryst. Solids **22**, 331 (1976).

[36] T .Tsuchiya, J. Phys. Soc. Jpn. **60**, 227 (1991).

[37] P. H. Poole, M. Hemmati and C. A. Angell, Phys. Rev. Lett. **79**, 2281 (1997).

[38] M. S. Shell, P. G. Debenedetti and A. Z. Panagiotopoulos, Phys. Rev. E **66**, 011202 (2002).

[39] R. Sharma, S. N. Chakraborty and C. Chakravarty, J. Chem. Phys. **125**, 204501 (2006).

[40] C. A Angell and H. Kano, Science **1121**, 193 (1976).

[41] S. Sastry and C. A. Angell, Nature Mater. **2**, 739 (2003).

[42] P. Vilaseca and G. Franzese, J. Non-Cryst. Solids **357**, 419-426 (2011).

[43] A. B. de Oliveira, E. B. Neves, C. Gavazzoni, J. Z. Paukowski, P. A. Netz and M. C. Barbosa, J. Chem. Phys. **132**, 164505 (2010).

[44] P. A. Netz, G. K. Gonzatti, M. C. Barbosa, J. Z. Paukowski, C. Gavazzoni and A. B. de Oliveira, *Thermodynamics - Physical Chemistry of Aqueous Systems* edited by Juan Carlos Moreno-Piraja, InTech Editors, New York, p. 291 (2011).

[45] D. B Hall, A. Dhinojwala and J. M. Torkelson, Phys. Rev. Lett. **79**, 103 (1997).

[46] M. T. Cicerone and M. D. Ediger, J. Chem. Phys. **104**, 7210 (1996).

[47] G. Sesé, J. O. Urbina and R. Palomar, J. Chem. Phys. **137**, 114502 (2012).

[48] H. J. C. Berendsen, and J. P. M. Postuma, and W. F. van Gunsteren, and A. DiNola, and J. R. Haak, J. Chem. Phys. **81**, 3684–3690 (1984).

[49] J. P. Ryckaert, G. Ciccotti and H. J. C. Berendsen, J. Comput. Phys. **23**, 327 (1977).

[50] See supplemental material at [URL] for informations about system equilibration.

[51] M. G. Noro and D. Frenkel, J. Chem. Phys. **113**, 8 (2000)

[52] G. Foffi and F. Sciortino, J. Phys. Chem. B **111** 9702-9705 (2007)

[53] N.V. Gribova, Yu. D. Fomin, D. Frenkel and V. N. Ryzhov, Phys. Rev. E **79**, 051202 (2009).

[54] Yu. D. Fomin, E. N. Tsiok and V. N. Ryzhov, J. Chem. Phys. **135**, 234502 (2011).

[55] Yu. D. Fomin, E. N. Tsiok and V. N. Ryzhov, Eur. Phys. J. Special Topics **216**, 165-173 (2013).

[56] Yu. D. Fomin, E. N. Tsiok and V. N. Ryzhov, Phys. Rev. E **87**, 042122 (2013).

[57] C. Vega, E. P. A. Paras and P. A. Monson, J. Chem. Phys. **97**, 8543 (1992).

[58] C. Vega and P. A. Monson, J. Chem. Phys. **107**, 2696 (1997).

[59] M. M. Szortyka, M. Girardi, V. B. Henriques and M. C. Barbosa, J. Chem. Phys. **132**, 134904 (2010).